

Coherent Terahertz Spin-Wave Emission Associated with Ferrimagnetic Domain Wall Dynamics

Se-Hyeok Oh,^{1,*} Se Kwon Kim,^{2,*} Dong-Kyu Lee,³ Gyungchoon Go,³ Kab-Jin Kim,^{4,5} Teruo Ono,⁵ Yaroslav Tserkovnyak,² and Kyung-Jin Lee^{1,3,6,†}

¹*Department of Nano-Semiconductor and Engineering, Korea University, Seoul 02841, Korea*

²*Department of Physics and Astronomy, University of California, Los Angeles, California 90095, USA*

³*Department of Materials Science and Engineering, Korea University, Seoul 02841, Korea*

⁴*Department of Physics, Korea Advanced Institute of Science and Technology, Daejeon 34141, Korea*

⁵*Institute for Chemical Research, Kyoto University, Kyoto 611-0011, Japan*

⁶*KU-KIST Graduate School of Converging Science and Technology, Korea University, Seoul 02841, Korea*

(Dated: December 3, 2021)

We theoretically study the dynamics of ferrimagnetic domain walls in the presence of Dzyaloshinskii-Moriya interaction. We find that an application of a DC magnetic field can induce terahertz spin-wave emission by driving ferrimagnetic domain walls, which is not possible for ferromagnetic or antiferromagnetic domain walls. Dzyaloshinskii-Moriya interaction is shown to facilitate the terahertz spin-wave emission in wide ranges of net angular momentum by increasing the Walker-breakdown field. Moreover, we show that spin-orbit torque combined with Dzyaloshinskii-Moriya interaction also drives a fast ferrimagnetic domain wall motion with emitting terahertz spin-waves in wide ranges of net angular momentum.

In modern communications, information is carried by electromagnetic waves of which frequency is limited to ≈ 0.1 terahertz (THz), the frequency of oscillating circuits based on high-speed transistors [1]. On the other hand, semiconductor lasers generate coherent light with the frequency > 30 THz [2]. Terahertz gap refers to the fact that no relevant technology exists in the frequency range between these two limits ($0.1 \sim 30$ THz). Therefore, it is of critical importance to find relevant physical phenomena that fill in the terahertz gap.

In this respect, antiferromagnets of which resonance frequencies are in the THz ranges [3, 4] are of interest [5, 6]. It has been reported that coherent THz magnons or spin-waves are generated in antiferromagnets, driven by a laser [7, 8] or an electrical current [9, 10]. However, THz spin-wave excitations by a DC magnetic field are in principle not possible for antiferromagnets as their magnetic moments are compensated on an atomic scale. In this work, we theoretically show that generation of coherent THz spin waves can be achieved by a field-driven domain wall (DW) motion in ferrimagnet/heavy metal bilayers in which the interfacial Dzyaloshinskii-Moriya interaction (DMI) is present.

As far as the terahertz gap is concerned, this DC field-driven scheme could be beneficial as it allows a low-power operation by avoiding laser-induced or current-induced heating. It is also fundamentally interesting as THz spin-wave emission is caused by an approximately relativistic dynamics of a ferrimagnetic DW. Relativistic kinematics refers to kinematics compatible with the theory of relativity [11], of which key ingredient is the Lorentz invariance with limiting velocity c , the speed of light. When the dispersion of a wave satisfies the Lorentz invariance, a quasiparticle corresponding to the wave follows an analogous relativistic kinematics with replacing

the speed of light by the maximum group velocity of the wave. When the velocity of quasiparticle approaches the maximum group velocity, it undergoes the Lorentz contraction and its speed saturates to the limiting velocity. An example of such quasiparticles is an antiferromagnetic DW [10, 12, 13]. When the DW velocity approaches the maximum spin-wave group velocity, the DW width shrinks with emitting spin-waves [10]. Similarly, the dynamics of a ferrimagnetic DW is also expected to exhibit the features of relativistic kinematics provided that the net magnetization and DMI, which break the Lorentz invariance of the system, are sufficiently ineffective.

In this Letter, we show that such an approximately relativistic DW dynamics is achievable for a class of ferrimagnets, rare earth (RE) and transition metal (TM) compounds, in which the spin moments are antiferromagnetically coupled. As RE and TM elements have different Landé- g factors [14], RE-TM ferrimagnets have two distinct temperatures; the magnetic moment compensation point T_M where net magnetic moment vanishes, and the angular momentum compensation point T_A where net angular momentum vanishes. For RE-TM ferrimagnets, resonance [15, 16], switching [17–21], domain wall motion [22–24], and skyrmion (or bubble domain) motion [25–27] near these compensation points have been explored experimentally and theoretically. In particular, an experimental observation of a fast field-driven DW motion at T_A in GdFeCo single-layered ferrimagnets was recently reported [23]. This observation reveals two distinguishing features of RE-TM ferrimagnets at T_A . One is that the spin dynamics is antiferromagnetic and thus fast because of zero net angular momentum at T_A . The other is that this fast antiferromagnetic dynamics is achieved by a field because the net magnetic moment is nonzero at T_A and thus couples with a magnetic field.

We begin with deriving the equations of motion for a ferrimagnetic DW based on the collective coordinate approach [28]. The dynamics of a general collinear ferromagnet at sufficiently low temperatures can be described by the following Lagrangian density [27, 29]

$$\mathcal{L} = \rho \dot{\mathbf{n}}^2/2 - \delta_s \mathbf{a}[\mathbf{n}] \cdot \dot{\mathbf{n}} - \mathcal{U}, \quad (1)$$

where \mathbf{n} is the unit vector along the collinear order, ρ parametrizes the inertia of the dynamics, δ_s is the spin density in the direction \mathbf{n} , $\mathbf{a}[\mathbf{n}]$ is the vector potential generated by a magnetic monopole of unit charge satisfying $\nabla_{\mathbf{n}} \times \mathbf{a} = \mathbf{n}$, and \mathcal{U} is the potential-energy density. Here, the first term is the spin Berry phase associated with the staggered spin density, which thus appears in the Lagrangian for collinear antiferromagnets; the second term is the Berry phase associated with the net spin density δ_s , which is used to describe the dynamics of uncompensated spins in ferrimagnets. We consider the following potential-energy density:

$$\begin{aligned} \mathcal{U} = & A(\nabla \mathbf{n})^2/2 - K(\mathbf{n} \cdot \hat{\mathbf{z}})^2/2 + \kappa(\mathbf{n} \cdot \hat{\mathbf{x}})^2/2 \\ & + D\hat{\mathbf{y}} \cdot (\mathbf{n} \times \partial_x \mathbf{n})/2 - \mathbf{h} \cdot \mathbf{n}. \end{aligned} \quad (2)$$

Here, the first term is the exchange energy with $A > 0$; the second term is the easy-axis anisotropy along the z axis with $K > 0$; the third term is the weaker DW hard-axis anisotropy along the x axis with $\kappa > 0$; the fourth term is the interfacial DMI; the last term is the Zeeman coupling with $\mathbf{h} = M\mathbf{H}$, where M is the net magnetization in the direction \mathbf{n} . The dissipation can be accounted for by introducing (the spatial density of) the Rayleigh dissipation function, $\mathcal{R} = s_\alpha \dot{\mathbf{n}}^2/2$. Here, s_α is a phenomenological parameter quantifying the energy and spin loss due to the magnetic dynamics. For example, in the ferromagnetic regime, i.e., away from T_A , it can be considered as the product of the effective Gilbert damping constant and the net spin density.

The low-energy dynamics of a DW can be described by the two collective coordinates, the position $X(t)$ and the azimuthal angle $\phi(t)$. We consider the Walker ansatz [30] for the DW profile: $\mathbf{n}(x, t) = (\sin \theta \cos \phi, \sin \theta \sin \phi, \cos \theta)$, where $\theta = 2 \tan^{-1} \{\exp[(x - X)/\lambda]\}$ and $\lambda = \sqrt{A/K}$ is the DW width. The equations of motion can be derived from Eqs. (1) and (2) in conjunction with the Rayleigh dissipation function:

$$M\ddot{X} + G\dot{\phi} + M\dot{X}/\tau = F, \quad (3)$$

$$I\ddot{\phi} - G\dot{X} + I\dot{\phi}/\tau = -\tilde{\kappa} \sin \phi \cos \phi + \tilde{D} \sin \phi, \quad (4)$$

where $M = 2\rho A/\lambda$ is the mass, $I = 2\rho A\lambda$ is the moment of inertia, $G = 2\delta_s A$ is the gyrotropic coefficient, $\tau = \rho/s_\alpha$ is the relaxation time, $F = 2hA$ is the force exerted by an external field, $\tilde{\kappa} = 2\kappa\lambda A$, $\tilde{D} = \pi D A/2$, and A is the cross-sectional area of the DW. From Eq. (3), we obtain the steady-state solution of the DW velocity:

$$V_{\text{DW}} = \frac{M\lambda}{s_\alpha} H, \quad (5)$$

where H is the external field applied along the z -axis. In this steady state, the DW moves at a constant velocity V_{DW} with a constant angle ϕ . When the field becomes sufficiently strong such that V_{DW} exceeds a certain threshold V_{max} , the DW begins to precess, engendering the phenomenon known as the Walker Breakdown [31, 32]. The Walker Breakdown field H_{WB} can be obtained from Eq. (4) by

$$H_{\text{WB}} = V_{\text{max}} \frac{s_\alpha}{M\lambda}. \quad (6)$$

In the absence of DMI ($D = 0$), the threshold velocity is given by $V_{\text{max}} = \tilde{\kappa}/2G$ and thus $H_{\text{WB}} = \tilde{\kappa}s_\alpha/2GM\lambda$. When DMI is much stronger than the DW anisotropy in the y direction, i.e., $|\tilde{D}| \gg \tilde{\kappa}$, then $|V_{\text{max}}| = |\tilde{D}|/G$. In this strong DMI limit, the Walker Breakdown field is given by

$$H_{\text{WB}} = \frac{|\tilde{D}|}{G} \frac{s_\alpha}{M\lambda} = \frac{\pi|D|}{4\delta_s} \frac{s_\alpha}{M\lambda}. \quad (7)$$

We note that H_{WB} is inversely proportional to G and thus to the net spin density δ_s . As a result, the Walker breakdown is absent at T_A where the net spin density vanishes, $\delta_s = 0$. This suppression of the Walker breakdown at T_A can be understood as a result of decoupling of the DW position X and the angle ϕ at T_A [23].

It is worthwhile comparing Eq. (7) to the Walker breakdown field for ferromagnetic DWs in the strong DMI limit [33]: $H_{\text{WB,FM}} = \alpha\pi D_{\text{FM}}/2M_{\text{FM}}\lambda_{\text{FM}}$, which can be obtained from Eq. (7) by taking the ferromagnetic limit. From this comparison, one finds that in the vicinity of T_A , H_{WB} for ferrimagnetic DWs is much larger than that for ferromagnetic DWs because $\delta_s \approx 0$ and $|M| \ll M_{\text{FM}}$. Moreover, this very large H_{WB} for ferrimagnetic DWs suggests that V_{DW} can reach the maximum group velocity of spin-wave more easily without experiencing the Walker breakdown and thus ferrimagnetic DWs can generate THz spin-waves in wide ranges of net angular momentum δ_s . Finally, the time averaged velocity \bar{V} for a one period far above the Walker Breakdown is given as

$$\bar{V} = \frac{M\lambda}{s_\alpha + \delta_s^2/s_\alpha} H. \quad (8)$$

To verify these theoretical predictions on the DW velocity and THz spin-wave emission, we perform atomistic model calculations [10, 34] for two-sublattice ferrimagnets, which correspond to RE-TM compounds. Two sublattices possess the magnetization M_1 and M_2 , which are coupled by the antiferromagnetic exchange. The spin densities are given by $s_1 = M_1/\gamma_1$ and $s_2 = M_2/\gamma_2$, where $\gamma_i = g_i\mu_B/\hbar$ is the gyromagnetic ratio of the lattice i , μ_B is the Bohr magneton, and g_i is the Landé-g factor. The parameters in the above descriptions for general ferrimagnets are given by $\delta_s = s_1 - s_2$, $M = M_1 - M_2$,

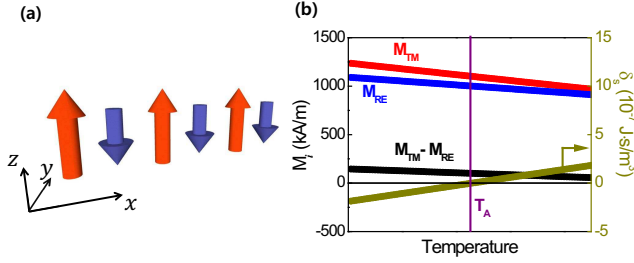


FIG. 1. (color online) (a) A schematic illustration of a ferrimagnet in which neighboring spins are coupled antiferromagnetically. (b) The assumed magnetic moments of TM (red) and RE (blue) elements as a function of the temperature T . Black symbols represent net magnetic moment ($= M_{TM} - M_{RE}$), and dark yellow symbols represent net angular momentum δ_s . Zero δ_s corresponds to the angular momentum compensation temperature T_A (purple). These parameters are used for simulations shown in Figs. 2 and 3.

and $s_\alpha = \alpha_1 s_1 + \alpha_2 s_2$, where α_i is the Gilbert damping constant for the lattice i . The one-dimensional discrete Hamiltonian that we use for numerical calculations is given by

$$\begin{aligned} \mathcal{H} = & A_{\text{sim}} \sum_i \mathbf{S}_i \cdot \mathbf{S}_{i+1} - K_{\text{sim}} \sum_i (\mathbf{S}_i \cdot \hat{\mathbf{z}})^2 \\ & + \kappa_{\text{sim}} \sum_i (\mathbf{S}_i \cdot \hat{\mathbf{x}})^2 + D_{\text{sim}} \sum_i \hat{\mathbf{y}} \cdot (\mathbf{S}_i \times \mathbf{S}_{i+1}) \\ & - g_i \mu_B \mu_0 \sum_i \mathbf{H} \cdot \mathbf{S}_i, \end{aligned} \quad (9)$$

where \mathbf{S}_i is the normalized spin moment vector at lattice site i [i.e., an even (odd) i corresponds to a RE (TM) atomic site], A_{sim} , K_{sim} , κ_{sim} , and D_{sim} denote the exchange, easy-axis anisotropy, DW hard-axis anisotropy, and DMI constants, respectively, and \mathbf{H} is the external field. We numerically solve the atomistic Landau-Lifshitz-Gilbert equation:

$$\frac{\partial \mathbf{S}_i}{\partial t} = -\gamma_i \mathbf{S}_i \times \mathbf{H}_{\text{eff},i} + \alpha_i \mathbf{S}_i \times \frac{\partial \mathbf{S}_i}{\partial t}, \quad (10)$$

where $\mathbf{H}_{\text{eff},i} = -\frac{1}{M_i} \frac{\partial \mathcal{H}}{\partial \mathbf{S}_i}$ is the effective field. We use the following simulation parameters: $A_{\text{sim}} = 30$ meV, $K_{\text{sim}} = 0.4$ meV, $\kappa_{\text{sim}} = 0.2$ μeV , damping constant $\alpha_{TM} = \alpha_{RE} = 0.002$, the lattice constant $d = 0.4$ nm, and Landé g -factors $g_{TM} = 2.2$ for TM, and $g_{RE} = 2$ for RE element [14]. Figure 1(b) shows the assumed temperature-dependent change in the magnetic moment M_i and corresponding δ_s . For simplicity, we assume other parameters are invariant with temperature.

Figure 2(a) shows V_{DW} for $D = 0$ as a function of H . Below H_{WB} , V_{DW} increases linearly with H , in agreement with Eq. (5) (solid lines). For $H > H_{WB}$, the Walker breakdown occurs except for $T = T_A$ at which V_{DW} keeps increasing because of the absence of the Walker breakdown, as explained above. Figure 2(b) shows H_{WB} as a function of δ_s at various DMIs. Two features are worth

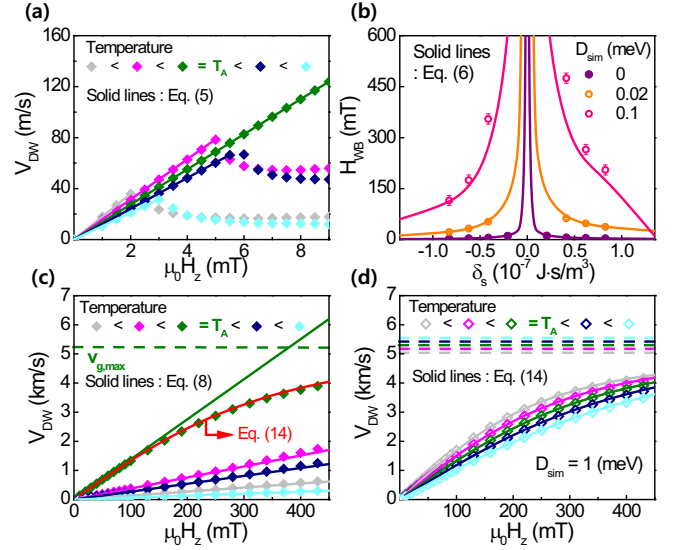


FIG. 2. (color online) (a) Domain wall velocity as a function of the external field H in the low-field regime ($\mu_0 H < 10$ mT). Symbols indicate the calculation results and solid lines indicate Eq. (5). (b) Walker Breakdown field H_{WB} as a function of net angular momentum δ_s at various DMI constants D_{sim} . Domain wall velocity in the high-field regime for (c) $D_{\text{sim}} = 0$ and (d) $D_{\text{sim}} = 1$ meV. Solid straight lines in (c) indicate Eq. (8). A red solid line in (c) and solid curved lines in (d) represent relativistically modified solution of domain wall velocity, Eq. (14). Horizontal dashed lines in (c) and (d) represent $v_{g,\text{max}}$ [Eq. (12)].

mentioning. First, H_{WB} diverges at T_A (i.e., $\delta_s = 0$). Second, H_{WB} for a finite DMI becomes much larger than that for $D = 0$, in agreement with Eq. (6) (solid lines). Compared to ferromagnets, ferrimagnets exhibit larger H_{WB} because the net magnetic moment $M (= M_1 - M_2)$ is small near T_A , as explained above. Figure 2(c) shows V_{DW} in the high field regime for $D = 0$. The numerically obtained values of V_{DW} at T_A (green symbols) deviate from Eq. (8) (a green solid line), which predicts a linear increase in V_{DW} with H . This deviation is a manifestation of the approximately relativistic dynamics of ferrimagnetic DW, as we will explain below in detail. For $D = 0$ [Fig. 2(c)], the nonlinear dependence of V_{DW} on H appears only at T_A . For $D_{\text{sim}} = 1$ meV (corresponding to $D = 2$ mJ/m²), however, the nonlinear dependence appears in all tested ranges of T [or δ_s ; Fig. 2(d)]. It means that the relativistic dynamics occurs in wide ranges of T , resulting from the largely enhanced H_{WB} near T_A .

For the cases showing the nonlinear dependence of V_{DW} on H , we observe the spin-wave emission from DW [Fig. 3(a)]. The spin-wave frequency is in THz ranges [Fig. 3(b)]. To elaborate the nonlinear dependence of V_{DW} on H and associated THz spin-wave emission, we derive the spin-wave dispersion for ferrimagnets on top of the uniform ground state, $\mathbf{n} = \hat{\mathbf{z}}$, given as

$$\omega_{\pm} = \frac{\pm \delta_s + \sqrt{\delta_s^2 + 4\rho(Ak^2 + K - h)}}{2\rho}, \quad (11)$$

where the upper (lower) sign corresponds to the right-handed (left-handed) circular mode and k is the wavenumber. We note that DMI does not contribute to the spin-wave dispersion as it is effective only for the y -component of magnetization, which is negligible for perpendicularly magnetized ferrimagnets. From the dispersion [Eq. (11)], we obtain the maximum spin-wave group velocity $v_{g,\max}$ as

$$v_{g,\max} = A/ds, \quad (12)$$

where $s = (s_1 + s_2)/2$. We note that $v_{g,\max}$ is indicated by horizontal dashed lines in Fig. 2(c) and (d). With $v_{g,\max}$, the nonlinear dependence of V_{DW} on H is readily interpreted based on the approximately relativistic kinematics of a DW, similar to the dynamics of an antiferromagnetic DW [10]: $v_{g,\max}$ acts as the speed of light [13] and the DW width shrinks as V_{DW} approaches $v_{g,\max}$ via the Lorentz contraction. The Lorentz contraction of DW is described by

$$\lambda_{\text{DW}} = \lambda_{\text{eq}} \sqrt{1 - (V_{\text{DW}}/v_{g,\max})^2}, \quad (13)$$

where λ_{eq} is the equilibrium DW width. The inertial DW mass also varies with the Lorentz factor $1/\sqrt{1 - (V_{\text{DW}}/v_{g,\max})^2}$, i.e., $M = 2\rho A/\lambda_{\text{DW}}$. Figure 3(c) shows that the DW width decreases as V_{DW} approaches $v_{g,\max}$ while the inertial mass increases with V_{DW} . With the Lorentz contraction, we modify Eq. (5) relativistically as

$$V_{\text{DW}} = v_{g,\max} \sqrt{1 - (\lambda_{\text{DW}}/\lambda_{\text{eq}})^2}, \quad (14)$$

which is represented by a red solid line in Fig. 2(c) and solid lines in Fig. 2(d). Excellent agreement between numerically obtained V_{DW} and Eq. (14) confirms the relativistic dynamics of ferrimagnetic DWs.

We also show that spin-orbit torque drives a fast relativistic motion of ferrimagnetic DWs. We consider damping-like torque only for simplicity. Using the collective coordinate approach, we obtain the steady-state solution of ferrimagnetic DW velocity as

$$V_{\text{DLT}} = \frac{\lambda_{\text{DW}} \pi s \tilde{B}_{\text{DLT}}}{2\alpha}, \quad (15)$$

where $\tilde{B}_{\text{DLT}} = \hbar \theta_{\text{SH}} J / 2et_z s_1 s_2$ is the effective field corresponding to the damping-like torque, θ_{SH} is the effective spin-Hall angle of ferrimagnet/heavy metal bilayer, J is the current density, e is the electron charge, and t_z is the ferrimagnet-thickness. Numerical simulation including the damping-like torque for $D_{\text{sim}} = 1$ meV [Fig. 3(d)] shows that spin-orbit torque combined with DMI effect is highly efficient for ferrimagnetic DW motion and the relativistic dynamics occurs for all tested ranges of T (or δ_s). This spin-orbit-torque-driven ferrimagnetic DW motion also accompanies with THz spin-wave emission (not shown).

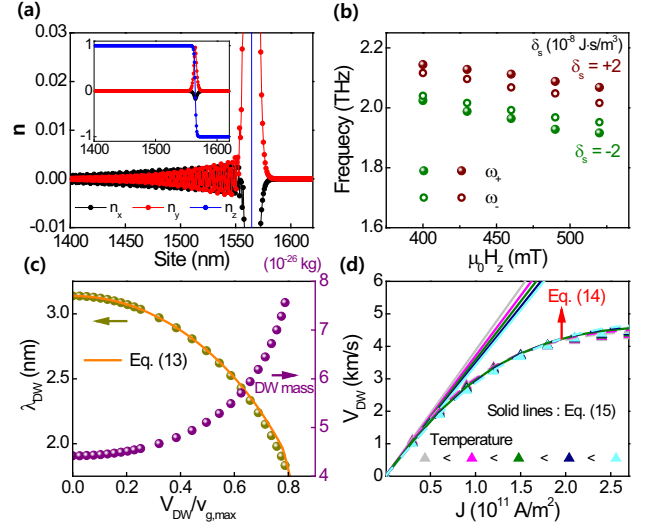


FIG. 3. (color online) (a) Configuration of domain wall and spin-waves for the staggered vector \mathbf{n} . The inset shows overall shape of domain wall. (b) The frequency of emitted spin-waves as a function of H with finite δ_s . ω_+ and ω_- indicate the right-handed and left-handed spin-wave modes, respectively [see Eq. (11)]. (c) Domain wall width and mass as a function of $V_{\text{DW}}/v_{g,\max}$ at T_A . The orange solid line indicates Eq. (13). (d) Domain wall velocity as a function of the current density J at several temperatures. Symbols represent calculation results and solid lines represent Eq. (15). Dashed lines represent relativistic modified solutions, Eq. (14).

Finally, we discuss about the origin of spin-wave emission from ferrimagnetic DWs. Two mechanisms have been proposed: Cherenkov-like process [35] and internal DW structure distortion [36]. The former occurs when DW velocity matches spin-wave phase velocity. In antiferromagnets or ferrimagnets near T_A , the phase velocity is always higher than the group velocity as one finds from the dispersion [Eq. (11)]. Therefore, this Cherenkov process is irrelevant to our case. For ferrimagnetic DWs, instead, the spin-waves can be emitted by releasing the DW energy enhanced through the Lorentz contraction as in the case of antiferromagnetic DWs [10].

In conclusion, we have shown field-driven THz spin-wave emission for ferrimagnetic DWs, which is not possible for ferromagnetic or antiferromagnetic DWs. In ferrimagnet/heavy metal bilayers in which the interfacial DMI arises naturally, the field-driven THz spin-wave emission can be observed in wide ranges of T (or δ_s), thereby largely enhancing the experimental accessibility to our prediction. Moreover, an in-plane current can also excite THz spin-waves in wide ranges of T (or δ_s) through the combined effect between spin-orbit torque and DMI. Our finding suggests that ferrimagnetic DWs are potentially useful for high-speed and high-frequency spintronics devices.

K.-J.L. was supported by the National Research Foundation of Korea (NRF) (NRF-2015M3D1A1070465, NRF-2017R1A2B2006119) and by the DGIST R&D Pro-

gram of the Ministry of Science, ICT and Future Planning (17-BT-02). S.K.K. and Y.T. were supported by the Army Research Office under Contract No. W911NF-14-1-0016. T.O. was supported by JSPS KAKENHI Grant Numbers 15H05702, 26103002. K.J.K. was supported by NRF-2017R1C1B2009686. G.G. was supported by NRF-2016R1A6A3A1193588.

* These two authors contributed equally to this work.

† kj_lee@korea.ac.kr

- [1] C. Sirtori, *Nature* **417**, 132 (2002).
- [2] M. Beck, D. Hofstetter, T. Aellen, J. Faist, U. Oesterle, M. Illegems, E. Gini, and H. Melchior, *Science* **295**, 301 (2002).
- [3] T. Nagamiya, *Prog. Theor. Phys.* **6**, 342 (1951).
- [4] F. Keffer and C. Kittel, *Phys. Rev.* **85**, 329 (1952).
- [5] T. Jungwirth, X. Marti, P. Wadley, and J. Wunderlich, *Nat. Nanotechnol.* **11**, 231 (2016).
- [6] V. Baltz, A. Manchon, M. Tsoi, T. Moriyama, T. Ono, and Y. Tserkovnyak, arXiv:1606.04284.
- [7] T. Satoh, S.-J. Cho, R. Iida, T. Shimura, K. Kuroda, H. Ueda, Y. Ueda, B. A. Ivanov, F. Nori, and M. Fiebig, *Phys. Rev. Lett.* **105**, 077402 (2010).
- [8] T. Kampftrath, A. Sell, G. Klatt, A. Pashkin, S. Mährlein, T. Dekorsy, M. Wolf, M. Fiebig, A. Leitenstorfer, and R. Huber, *Nat. Photonics* **5**, 31 (2011).
- [9] R. Cheng, D. Xiao, and A. Brataas, *Phys. Rev. Lett.* **116**, 207603 (2016).
- [10] T. Shiino, S.-H. Oh, P. M. Haney, S.-W. Lee, G. Go, B.-G. Park, and K.-J. Lee, *Phys. Rev. Lett.* **117**, 087203 (2016).
- [11] A. Einstein, *Annalen der physik* **322**, 891 (1905).
- [12] F. D. M. Haldane, *Phys. Rev. Lett.* **50**, 1153 (1983).
- [13] S. K. Kim, Y. Tserkovnyak, and O. Tchernyshyov, *Phys. Rev. B* **90**, 104406 (2014).
- [14] J. Jensen and A. R. Mackintosh, *Rare earth magnetism* (Clarendon Oxford, 1991).
- [15] M. Binder, A. Weber, O. Mosendz, G. Woltersdorf, M. Izquierdo, I. Neudecker, J. R. Dahn, T. D. Hatchard, J.-U. Thiele, C. H. Back, and M. R. Scheinfein, *Phys. Rev. B* **74**, 134404 (2006).
- [16] C. D. Stanciu, A. V. Kimel, F. Hansteen, A. Tsukamoto, A. Itoh, A. Kiriliyuk, and T. Rasing, *Phys. Rev. B* **73**, 220402 (2006).
- [17] N. Roschewsky, T. Matsumura, S. Cheema, F. Hellman, T. Kato, S. Iwata, and S. Salahuddin, *Appl. Phys. Lett.* **109**, 112403 (2016).
- [18] X. Jiang, L. Gao, J. Z. Sun, and S. S. P. Parkin, *Phys. Rev. Lett.* **97**, 217202 (2006).
- [19] J. Finley and L. Liu, *Phys. Rev. Applied* **6**, 054001 (2016).
- [20] K. Ueda, M. Mann, C.-F. Pai, A.-J. Tan, and G. S. Beach, *Appl. Phys. Lett.* **109**, 232403 (2016).
- [21] R. Mishra, J. Yu, X. Qiu, M. Motapothula, T. Venkatesan, and H. Yang, *Phys. Rev. Lett.* **118**, 167201 (2017).
- [22] T. Tono, T. Taniguchi, K.-J. Kim, T. Moriyama, A. Tsukamoto, and T. Ono, *Appl. Phys. Express* **8**, 073001 (2015).
- [23] K.-J. Kim, S. K. Kim, T. Tono, S.-H. Oh, T. Okuno, W. S. Ham, Y. Hirata, S. Kim, G. Go, Y. Tserkovnyak, A. Tsukamoto, T. Moriyama, K.-J. Lee, and T. Ono, arXiv:1703.07515 (2017).
- [24] H. Awano, *J. Magn. Magn. Mater.* **383**, 50 (2015).
- [25] M. Tanaka, H. Kanazawa, S. Sumitomo, S. Honda, K. Mibu, and H. Awano, *Appl. Phys. Express* **8**, 073002 (2015).
- [26] M. Tanaka, S. Sumitomo, N. Adachi, S. Honda, H. Awano, and K. Mibu, *AIP Advances* **7**, 055916 (2017).
- [27] S. K. Kim, K.-J. Lee, and Y. Tserkovnyak, *Phys. Rev. B* **95**, 140404(R) (2017).
- [28] O. A. Tretiakov, D. Clarke, G.-W. Chern, Y. B. Bazaliy, and O. Tchernyshyov, *Phys. Rev. Lett.* **100**, 127204 (2008).
- [29] A. F. Andreev and V. I. Marchenko, *Sov. Phys. Usp.* **23**, 21 (1980).
- [30] L. D. Landau and E. M. Lifshitz, *Electrodynamics of Continuous Media*, Course of Theoretical Physics Vol. 8 (Pergamon, Oxford, 1960).
- [31] N. L. Schryer and L. R. Walker, *J. Appl. Phys.* **45**, 5406 (1974).
- [32] A. Mougin, M. Cormier, J. Adam, P. Metaxas, and J. Ferr, *Europhys. Lett.* **78**, 57007 (2007).
- [33] A. Thiaville, S. Rohart, É. Jué, V. Cros, and A. Fert, *Europhys. Lett.* **100**, 57002 (2012).
- [34] R. F. Evans, W. J. Fan, P. Chureemart, T. A. Ostler, M. O. Ellis, and R. W. Chantrell, *J. Phys.: Condens. Matter* **26**, 103202 (2014).
- [35] M. Yan, C. Andreas, A. Kákay, F. García-Sánchez, and R. Hertel, *Appl. Phys. Lett.* **99**, 122505 (2011).
- [36] X. S. Wang, P. Yan, Y. H. Shen, G.E.W. Bauer, and X. R. Wang, *Phys. Rev. Lett.* **109**, 167209 (2012).